High Up-Conversion Efficiency of YVO_4:Yb,Er Nanoparticles in Water down to the Single-Particle Level

Geneviève Mialon,[†] Silvan Türkcan,[‡] Géraldine Dantelle,*[,†] Daniel P. Collins,[§] Maria Hadjipanayi,[§] Robert A. Taylor,[§] Thierry Gacoin,[†] Antigoni Alexandrou,[‡] and Jean-Pierre Boilot[†]

Laboratoire de Physique de la Matière Condensée - CNRS UMR 7643 - Ecole Polytechnique, Route de Saclay, 91128 Palaiseau Cedex, France, Laboratoire d'Optique et Biosciences - CNRS UMR 7645, INSERM U696 - Ecole Polytechnique, Route de Saclay, 91128 Palaiseau Cedex, France, and Clarendon Laboratory, Department of Physics, University of Oxford, OX1 3PU Oxford, United Kingdom

Received: August 20, 2010; Revised Manuscript Received: October 25, 2010

We report up-conversion emission from an aqueous solution of YVO_4:Yb^{3+},Er^{3+} nanocrystals synthesized by an original method that produces nanoparticles with excellent crystallinity and no porosity. We show that these YVO_4:Yb^{3+},Er^{3+} nanocrystals are not very sensitive to nonradiative relaxations, leading to a high green-to-red emission ratio of 6.3. Using a comparison with YVO_4:Eu^{3+} particles, we determined the quantum yield of the up-conversion emission of the aqueous YVO_4:Yb^{3+},Er^{3+} dispersion to be $0.09 \pm 0.04\%$ for an excitation intensity of only 0.55 kW·cm^{-2} at 970 nm. Furthermore, single YVO_4:Yb,Er particles with an estimated size down to 10 nm can be detected using a wide-field microscope under a 970 nm, 8 kW·cm^{-2} excitation. Because of their unexpectedly high up-conversion emission without intermittency, their water dispersibility, and their photostability, YVO_4:Yb^{3+},Er^{3+} nanoparticles are highly appropriate both for single-biomolecule and for in vivo imaging.

Introduction

Over the past decade, various types of inorganic nanoparticles have been developed for their use as fluorescent probes in biomedical imaging.[1,2] So far, most systems exhibit light emission properties in the visible range through usual down-conversion of the excitation energy. An important limitation is that light in this wavelength range is absorbed by surrounding biological species. This leads to background fluorescence, decreasing the signal-to-noise ratio and affecting the quality of the fluorescence imaging. It also limits the penetration depth of the excitation, thus limiting in vivo imaging. Furthermore, the excitation beam may damage the biological environment near the probes.

To overcome these drawbacks, many studies aim at developing systems that may be used in the spectral window of relative transparency of biological tissues that lies in the NIR region. Several studies have concentrated on semiconductor quantum dots (QDs), for example, InP or PbS.[3] However, development of imaging in the NIR spectral range is somewhat limited by the availability of commercial detectors of sufficient sensitivity in this spectral region. In this context, the nonlinear emission in the visible range after excitation in the NIR of particles, in particular QDs, has been exploited (two-photon absorption[4] or second-harmonic generation emission[5]). The additional advantage in this case is that nonlinear emission processes provide optical sectioning capability.[6]

Up-conversion phosphor particles, typically Yb^{3+}- and Er^{3+}-doped oxides or fluorides, are clearly of interest in this context. Indeed, up-conversion processes, based on sequential discrete absorptions and energy transfers between doping ions,[7,8] allow generation of visible photons under NIR excitation. Because these up-conversion processes involve real long-lived metastable states with lifetimes on the microsecond scale, they are extremely efficient compared to multiphoton processes involving virtual states. Up-conversion luminescence can thus be excited with continuous-wave (CW) lasers, whereas multiphoton excitation typically requires expensive, pulsed lasers. Up-conversion luminescence upon NIR excitation thus combines the advantages of negligible cell or tissue background fluorescence, deep penetration, low scattering of the excitation, low photodamage, and use of cheap CW lasers.

Furthermore, lanthanide-doped nanoparticles are detectable at the single-particle level, as we demonstrated for Eu-doped YVO_4 particles,[9,10] and show no emission intermittency,[9,10] in contrast to standard QDs, which is an important advantage for single-biomolecule tracking applications. We could thus obtain extremely long, uninterrupted trajectories of membrane receptors using a wide-field microscope.[11]

Up-conversion fluorescence is commonly observed in bulk materials with relatively low phonon energy, such as in fluoride matrixes, as up-conversion processes are very sensitive to nonradiative multiphonon relaxations.[12,13] Bulk β-$NaYF_4$:Er^{3+},Yb^{3+} (with a phonon energy cutoff of $\nu_{NaYF4} \sim 350$ cm^{-1}) is known as the most efficient up-conversion crystal.[14] As far as nanomaterials are concerned, several systems have been investigated, mostly on dry powders (LaF_3,[15] PbF_2,[16] Y_2O_3,[17] YVO_4[18]) or on nanoparticles dispersed in a glassy or polymer matrix.[19,20] Far fewer studies concerned the study of up-conversion in nanoparticles dispersed in solution because no up-conversion signal can usually be detected in this case. Indeed,

* To whom correspondence should be addressed. E-mail: geraldine.dantelle@polytechnique.edu.
[†] Laboratoire de Physique de la Matière Condensée - CNRS UMR 7643 - Ecole Polytechnique.
[‡] Laboratoire d'Optique et Biosciences - CNRS UMR 7645, INSERM U696 - Ecole Polytechnique.
[§] University of Oxford.

10.1021/jp107900z
Published on Web 12/02/2010

because of the implication of intermediate excited states of low energy, up-conversion is highly sensitive to nonradiative processes that occur in nanoparticles due to the presence of adsorbed species or defects inherent to their small size and low synthesis temperature. The role of the adsorbed species is all the more important given that the specific surface area in these systems is very high and that biolabeling applications require dispersions of the particles into water, resulting in surface groups that are very efficient quenchers of the excited states (OH, PEGs, surfactants, or appropriate acids[21]).

To our knowledge, the only reported up-conversion studies in colloidal dispersions concern β-$NaYF_4$ and β-$NaGdF_4$ nanoparticle dispersions. Er^{3+}- and Yb^{3+}-doped nanoparticles display relatively strong up-conversion luminescence, but only when dispersed in aprotic organic solvents (in DMSO,[22−24] in cyclohexane,[25] in hexane[26]), which eliminate the drastic effect of quenching, by hydroxyl groups. As compared with the related bulk material, β-$NaYF_4$ or β-$NaGdF_4$ nanocrystals display an up-conversion efficiency that is typically 10^1-10^3 times weaker because of the presence of surface organic ligands in proximity to Ln^{3+} ions.[22,23,26] The application of the core/shell strategy in order to increase the distance between the Ln^{3+} ions and the surface of the particles allowed G. Yi and G. Chow to improve, by a factor of 7, the emission yield of $NaYF_4$:Yb,Er/$NaYF_4$ as compared with the bare nanoparticles.[27]

Our aim was to test other compositions that may not be optimal as far as phonon frequency of the host matrix is concerned, but whose synthesis is very well controlled, leading to particles with excellent crystallinity and whose size (20−40 nm) is large enough to limit surface quenching even in aqueous dispersions. We have recently produced YVO_4 nanoparticles with an excellent crystallinity through annealing at 1000 °C, using a process that allows the recovery of well-dispersed particles with the same size as an aqueous colloidal suspension.[28] Down-conversion emission from Eu^{3+} in YVO_4 particles was found to be drastically improved, similar to that of the bulk material and limited only by dielectric confinement effects intrinsic to the small size and dispersion in water that has a lower refractive index than bulk YVO_4.[29]

On the basis of these results, this paper describes a similar strategy to produce aqueous dispersions of annealed up-conversion YVO_4:Yb,Er nanoparticles. The idea was to obtain particles for which the detrimental effect of a higher phonon energy of the vanadate matrix (in bulk, $\nu_{YVO4} \sim 890\ cm^{-1}$,[30] as compared with fluorides, $\nu_{NaYF4} \sim 350\ cm^{-1}$) would be counterbalanced by their exceptional crystallinity and optimized emission properties. The application of these nanoparticles as original biological labels is straightforward given that functionalization and coupling to biomolecules has already been addressed in the case of YVO_4:Eu nanoparticles.[31,32]

We observed an unexpectedly high up-conversion emission from these particles in water, with a green-to-red ratio as high as 6.3 and a quantum efficiency of 0.09 ± 0.04% for an excitation intensity of only 0.55 $kW \cdot cm^{-2}$. In addition, we report the up-conversion emission of single YVO_4:Er,Yb nanoparticles deposited on a glass coverslip and covered with water with estimated sizes down to 10 nm for an excitation intensity as low as 8 kW/cm^2 at 970 nm in a wide-field setup. These particles do not blink and are highly photostable. Their excitation in the near-IR is particularly favorable for biological applications because the cell and tissue absorption in this wavelength range is very low. The absence of background cell fluorescence and high penetration depths in tissues can thus be obtained. These up-converting YVO_4:Yb,Er nanoparticles are thus highly suitable both for single-molecule tracking in cells and for imaging in tissues.

Experimental Methods

Synthesis. A solution of $Y(NO_3)_3$, $Er(NO_3)_3$, and $Yb(NO_3)_3$ (c = 0.1, 0.002, and 0.02 mol/L, respectively) is slowly added to a Na_3VO_4 solution (c = 0.1 mol/L) under constant stirring, at room temperature. A white precipitate, corresponding to crude YVO_4:Er,Yb nanoparticles is obtained and further purified by dialysis. A silica sol is prepared by heating tetraethylorthosilicate (TEOS), ethanol, and distilled water at pH = 1.25 at 60 °C for 1 h. The crude yttrium orthovanadate particles are then incorporated into a silica sol with a dispersing polymer (PE6800), with the molar ratio of V/Si/PE6800 = 1:5:0.05. After drying, a mesoporous silica network is obtained, encapsulating the nanoparticles. It is calcinated at 500 °C for 1 h and then annealed at 1000 °C for 10 min. The silica matrix is removed by a 3 h treatment in hydrofluoric acid with the molar ratio of HF/Si = 9:1. The YVO_4:Eu nanoparticles were synthesized as discussed in ref 33.

Electron Microscopy Characterization. Scanning electron microscopy images were obtained using a FEG-SEM Hitachi 4800 operating at 5 kV, 5 μA. The solution was spin-coated on a Si substrate and a 10 nm Au layer was deposited on the substrate to avoid charging effects.

Ensemble Emission Measurements. The colloidal solutions of YVO_4:Eu and YVO_4:Er,Yb nanoparticles were excited using, respectively, the 466 nm Argon laser line and a 975 nm laser diode (ThorLabs, L975P1WJ) filtered by a pair of 700 nm long-pass filters (720 LP). In the experiments for the quantum yield determination, the emission of the nanoparticles was detected by a PMT (Hamamatsu R636-10) and an oscilloscope (Tektronix TDS 3032) at an angle of 90° after filtering out the laser emission either by using a band-pass filter (Chroma D 617/8M) for Eu-doped particles or by using a low-pass filter (Chroma E700SP) for YVO_4:Er,Yb.

Emission spectra of the solutions in the visible were recorded at room temperature with a Jobin-Yvon H25 spectrometer and a liquid-nitrogen-cooled CCD camera (Princeton Instruments LN/CCD-400-PB, 400 × 1340 pixels, back-illuminated).

Emission spectra of the nanoparticles in powder were recorded using a microphotoluminescence setup: The excitation was done via a microscope objective, using a CW Ti:Sapphire laser centered at 960 nm. The emission was detected, via the objective, by a spectrometer (0.3 m Andor Shamrock) equipped with an InGaAs array detector (Andor DU490A 1.7) for the 1.5 μm emission or with a CCD camera (Andor 420 BU) for the visible emission. Thanks to this setup, emission spectra in the visible range and at 1.5 μm can be recorded without moving the sample. Both spectral measurement setups were calibrated using blackbody radiation. Thus, quantitative information on the relative emission in these ranges can be achieved.

Lifetime Measurements. Fluorescence decay measurements were performed under pulsed excitation using an optical parametric oscillator (OPO), pumped by the third harmonic of a Q-switched Nd^{3+}−YAG laser (355 nm). The fluorescence at 1.5 μm was detected with an InGaAs detector and visualized onto a digital oscilloscope (TDS 350 Tektronix).

Single-Particle Microscopy. We used a wide-field inverted microscope (Zeiss Axiovert 100) equipped with a 60×, N.A. = 1.35 NIR-transmitting oil immersion objective (Olympus UPlanSApo). The YVO_4:Yb,Er nanoparticles, deposited onto a microscope coverslip and covered with a water droplet, were

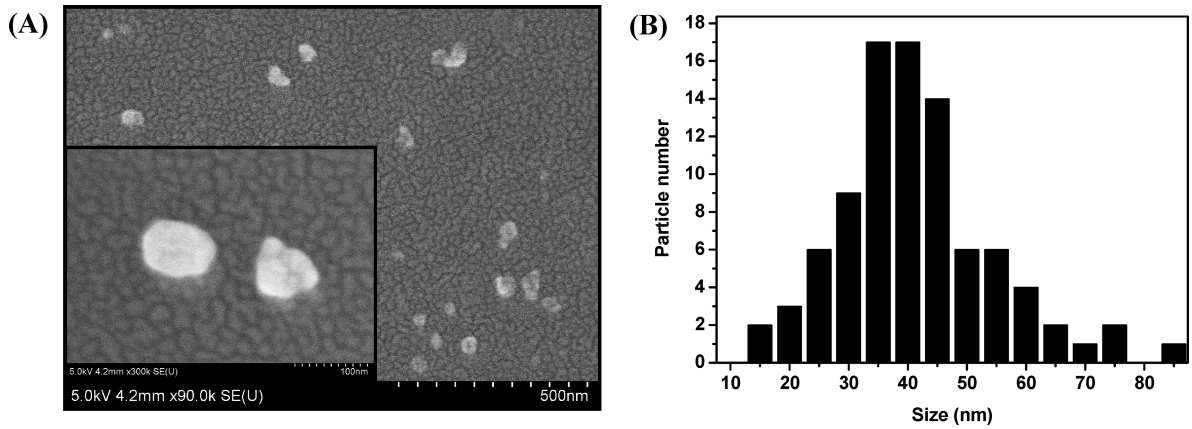

Figure 1. (A) SEM images of YVO_4 nanoparticles doped with Er^{3+} and Yb^{3+}. The granular aspect is given by the presence of a 10 nm Au layer, deposited on the substrate to avoid charging effects. (B) Size distribution of the nanoparticles.

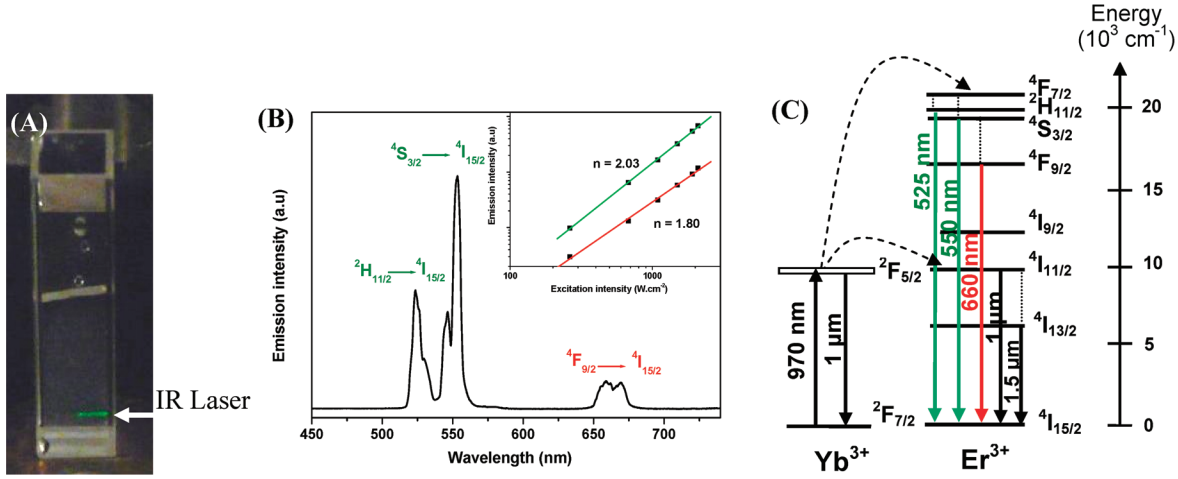

Figure 2. (A) Photograph of a 0.2 wt % transparent colloidal solution of YVO_4:20%Yb,2%Er nanocrystals in water under 970 nm excitation with a diode laser of about 2 kW·cm^{-2}. The excitation laser (780 mW) was focused at the entrance of the vial down to 220 μm. The excitation intensity progressively decreases to 0 inside the vial due to absorption by the nanoparticle solution. (B) Corresponding up-conversion spectrum. Inset: dependence of the green ($^4S_{3/2}$−$^4I_{15/2}$) and red ($^4F_{9/2}$−$^4I_{15/2}$) luminescence intensities of the colloidal YVO_4:20%Yb,2%Er solution as a function of the excitation power in double logarithmic representation. The solid lines are least-squares fits to the data with slopes of 2.03 ± 0.05 and 1.80 ± 0.08 for the green and red emission intensities, respectively. (C) Schematic energy-level diagram showing energy transfers in the Yb^{3+},Er^{3+} system. Full, dashed, and dotted arrows indicate radiative processes, energy transfers, and multiphonon relaxations, respectively.

excited with a 975 nm laser diode (ThorLabs, L975P1WJ) filtered by a pair of 700 nm long-pass filters (720 LP). The FWHM of the excitation beam was 82 μm with a maximal excitation intensity of 8 kW·cm^{-2}. The emission of the nanoparticles was collected through a dichroic mirror (Omega 675DCSPXR) and a low-pass filter (Chroma E700SP). Images were recorded with an EM-CCD (Roper Scientific QuantEM: 512SC).

Results and Discussion

Structural Characterization. The procedure to synthesize our Yb^{3+} and Er^{3+}-doped YVO_4 nanoparticles consists of the following: (1) the coprecipitation of vanadate and yttrium salts in water (pH > 11) at room temperature, (2) the incorporation of the nanoparticles in a porous silica matrix to avoid particle sintering, (3) the annealing of the composite material at 1000 °C, and (4) the removal of the silica by an HF treatment to recover the annealed particles. Details on the structural evolution of the particles during the annealing treatment are reported in our previous papers.[28,29]

The obtained YVO_4:Yb,Er nanoparticles are easily dispersible in water, forming a stable colloidal solution. Their size distribution obtained from scanning electron microscopy images (SEM) (Figure 1A) peaks at 39 nm (σ = 17 nm) (Figure 1B).

Up-Conversion Emission in Water. Upon 970 nm excitation of the aqueous solution of Yb,Er-doped YVO_4 nanoparticles, green up-conversion luminescence was observed by the naked eye (Figure 2A). The corresponding emission spectrum is presented in Figure 2B. A strong emission band situated around 525−550 nm is seen, together with a weaker band in the red region.

Up-conversion luminescence can result from different mechanisms (energy transfer up-conversion, excited-state absorption, photon avalanche), widely described in the literature.[7,8] All of them are characterized by multiple energy transfers between the sensitizer and the activator (here, Yb^{3+} and Er^{3+}, respectively). Figure 2C shows the energy transfer up-conversion mechanism: (1) after absorption of a NIR photon by Yb^{3+}, energy transfer from the excited ($^2F_{5/2}$) Yb^{3+} to Er^{3+} promotes Er^{3+} to the quasi-resonant metastable $^4I_{11/2}$ level, and (2) absorption of a second NIR photon by Yb^{3+} and energy transfer from this excited ($^2F_{5/2}$) Yb^{3+} to the previously excited ($^4I_{11/2}$) Er^{3+} promotes Er^{3+} to the $^4F_{7/2}$. The two main emission lines centered at 525 nm (19 050 cm^{-1}) and 550 nm (18 100 cm^{-1}) correspond respectively to the radiative $^2H_{11/2} \rightarrow {}^4I_{15/2}$ and $^4S_{3/2}$

TABLE 1: Green-to-Red Ratio of Different Nanoparticles in Water[d]

nanoparticles	GRR value	ref
HEDP-modified $NaYF_4$:Yb,Er	0.154[a]	21
PAA-coated $NaYF_4$:Yb,Er/α-$NaYF_4$ core/shell	2[b]	26
YVO_4:Yb,Er	6.3[c]	this work

[a] The excitation intensity was 150 $W \cdot cm^{-2}$. [b] The excitation intensity was 15 $W \cdot cm^{-2}$. [c] The excitation intensity was 2 $kW \cdot cm^{-2}$. [d] HEDP and PAA stand for 1-hydroxyethane-1,1-diphosphonic acid and poly(acrylic acid), respectively. Note that $NaYF_4$ nanocrystals need to be functionalized to be water-soluble. Note that, for YVO_4 nanoparticles, for an excitation intensity varying from 0.2 to 2 $kW \cdot cm^{-2}$, similar GRR values were found.

$\rightarrow {}^4I_{15/2}$ transitions of Er^{3+}. The red emission peaking at 660 nm (15 200 cm^{-1}) arises from the ${}^4F_{9/2}-{}^4I_{15/2}$ transition. The two-photon excitation process leading to this visible emission is demonstrated by examining the dependence of the intensity of the green and red emission bands as a function of the excitation intensity: the intensity of these emission bands indeed varies as the second power of the excitation (Figure 2B, inset).

An indirect, though common, way to evaluate the up-conversion efficiency of a system consists of calculating the intensity ratio between the integrated emission bands centered at about 525−550 nm and at 660 nm, called the green-to-red ratio (usually designated GRR).[34−38] The ${}^4F_{9/2}$ level, giving rise to the red emission, is populated from the ${}^2H_{11/2}$ and ${}^4S_{3/2}$ levels, either by nonradiative multiphonon relaxations or by cross-relaxations between neighboring Er^{3+} ions.[39,40] A low GRR is observed if fast nonradiative pathways (multiphonon relaxations or cross-relaxations) occur from the ${}^2H_{11/2}$ and ${}^4S_{3/2}$ levels to the ${}^4F_{9/2}$ level. The presence of fast nonradiative relaxations will also shorten the lifetime of the ${}^4I_{11/2}$ excited state, the intermediate level for the up-conversion process, and will consequently lead to the reduction of the up-conversion emission.[41] Thus, it is common to consider that particles with a low GRR value (i.e., a strong red emission with respect to the green emission) also have a weak up-conversion efficiency and vice versa.[21]

In the literature, very few measurements of the GRR of nanoparticles in water have been reported (see Table 1). After optimization of the Er and Yb contents, we measured a GRR of 6.3 for YVO_4:2%Er:20%Yb in water ($\lambda_{exc} = 970$ nm), which is much higher than the GRR value of 0.154 reported for an aqueous solution of $NaYF_4$:Yb,Er particles coated with a phosphonic acid (HEDP) to obtain water solubility and the GRR value of 2 reported for a core/shell system ($NaYF_4$:Yb,Er/α-$NaYF_4$) coated with a poly(acrylic acid). The GRR value of the core/shell system is higher than the one of HEDP-modified $NaYF_4$:Yb,Er particles because the α-$NaYF_4$ shell protects the active core from surface groups, responsible for efficient nonradiative relaxations. However, YVO_4:Yb,Er nanocrystals are much less affected by nonradiative multiphonon relaxations than both these $NaYF_4$:Yb,Er particles, probably because of the high crystallinity that characterizes YVO_4 particles after the thermal treatment.[29]

Indeed, we ascribe this difference to the fact that our YVO_4:Yb,Er particles are less sensitive to −OH or organic quenchers because of their reduced porosity,[29] which limits the number of adsorption sites, and to the fact that they contain fewer lattice defects because of their high crystallinity.[28,29] YVO_4:Yb,Er nanoparticles obtained by this original thermal annealing process thus appear as a very competitive material for efficient up-conversion fluorescence in water.

Up-Conversion Emission versus Direct NIR Emission. The up-conversion luminescence of YVO_4:Yb,Er nanoparticles was then compared to the direct luminescence of Er^{3+} at 1.5 μm, corresponding to the ${}^4I_{13/2} \rightarrow {}^4I_{15/2}$ transition (Figure 3). This experiment could not be performed in water, which absorbs the 1.5 μm radiation. Therefore, dry YVO_4:Yb,Er nanoparticles were deposited on a glass substrate. Using a microphotoluminescence setup, they were excited by a CW Ti:sapphire laser at 960 nm with an intensity of 12 $kW \cdot cm^{-2}$. Figure 3 shows the emission spectrum, with assignment of the emission bands, in the visible and in the NIR range. The optical setup was calibrated, allowing the direct comparison of the emission intensities. In these conditions, the up-conversion emission is 4 times stronger than the 1.5 μm emission.

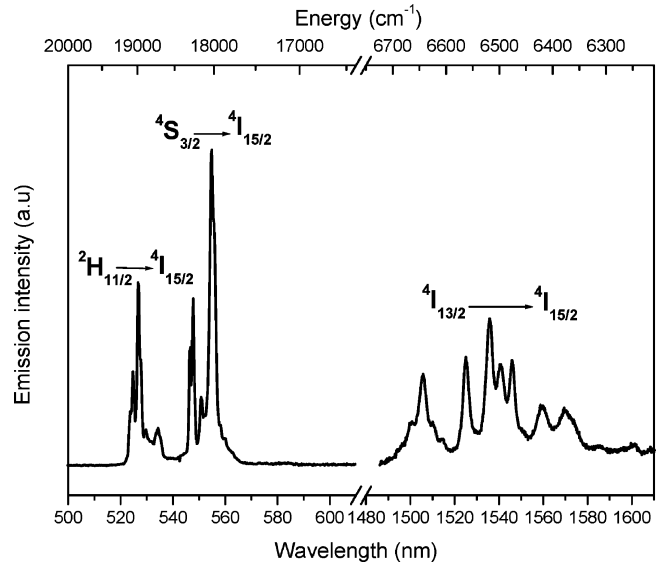

Figure 3. Emission spectrum of YVO_4:20%Yb,2%Er nanoparticles deposited on a glass substrate and excited by a CW Ti:sapphire laser at 960 nm with an intensity of 12 $kW \cdot cm^{-2}$. The spectra are corrected for the setup detection efficiency in the visible and in the NIR range.

The ${}^4I_{13/2}$ level, responsible for the 1.5 μm emission, is mainly populated by nonradiative de-excitations from the ${}^4I_{11/2}$ level, which is also the intermediate level for the up-conversion processes (Figure 2C). The weak emission at 1.5 μm with respect to the up-conversion emission reflects the weak contribution of nonradiative relaxation processes from the ${}^4I_{11/2}$ to the ${}^4I_{13/2}$ level, leading to a relatively long lifetime of the intermediate ${}^4I_{11/2}$ state, at least long enough for up-conversion to occur. Hence, this confirms that the luminescence of YVO_4:Yb,Er nanoparticles is only weakly affected by crystalline defects or high-energy phonons, responsible for the depletion of the ${}^4I_{11/2}$ level.

Lifetime Measurements. The fluorescence decay curve of YVO_4:20%Yb:2%Er nanoparticles was recorded at 1.5 μm (corresponding to the ${}^4I_{13/2}-{}^4I_{15/2}$ transition) under a 980 nm excitation (i.e., mainly into the ${}^4I_{11/2}$ level of Er^{3+}). From the rise time of the 1.5 μm emission, we can estimate that the ${}^4I_{11/2}$ level lifetime is $\tau({}^4I_{11/2}) \sim 20$ μs. The ${}^4I_{13/2}$ lifetime is measured to be $\tau({}^4I_{13/2}) = 1.4$ ms. In bulk YVO_4:2.5%Er, the ${}^4I_{11/2}$ and ${}^4I_{13/2}$ lifetimes are reported to be 31.65 μs and 2.4 ms, respectively.[42] This comparison shows that excited-level lifetimes of Er^{3+} in the annealed YVO_4 nanoparticles are similar to those obtained in bulk YVO_4 and much longer than those obtained in nonannealed YVO_4 nanoparticles: $\tau({}^4I_{13/2}) = 25$ μs,[43] further confirming our assumption that the annealed nanoparticles have a limited number of defects.

Up-Conversion Quantum Yield. We then went on to estimate the quantum yield of the up-conversion emission of

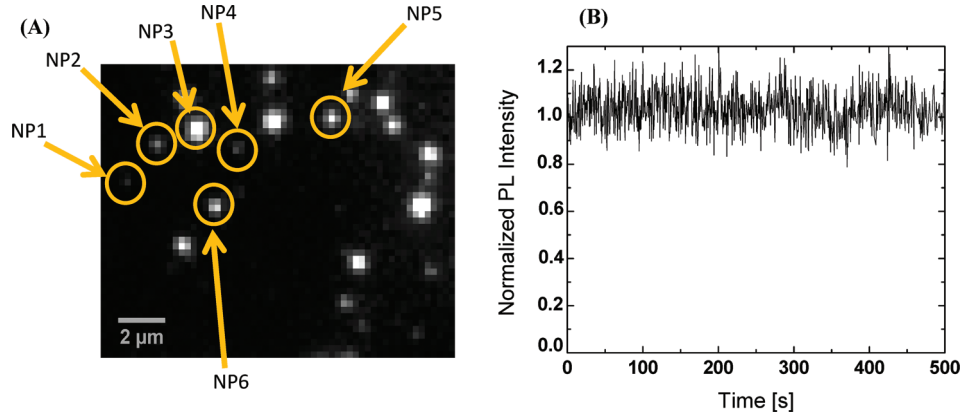

Figure 4. (A) Wide-field fluorescence microscopy of YVO_4 nanoparticles deposited on a glass coverslip and covered by a water drop. The excitation power was 8 kW·cm^{-2} and the integration time 500 ms. (B) Photostability of a single up-converting nanoparticle under CW 970 nm excitation.

these particles defined as the ratio of emitted up-converted photons to absorbed NIR photons. There are very few determinations of the up-conversion quantum yield in the literature.[44,45] For the two-photon up-conversion effect, it is indeed difficult to obtain conditions compatible with quantum yield measurements (dilute, weakly absorbing solutions, homogeneous excitation intensity throughout the sample) while maintaining a measurable up-conversion signal. We, here, compared the up-conversion emission with the emission of nonannealed YVO_4:Eu particles, used at the single-particle level for biological applications.[9,46,47] The comparison was performed on dilute aqueous colloidal solutions with a vanadium content of 4.3 and 2.1 mM for the YVO_4:Eu and the YVO_4:Yb,Er solutions, respectively, to ensure negligible absorption of the excitation beam. The excitation laser was loosely focused to obtain a quasi-constant excitation intensity throughout the 2 mm vial, and the luminescence was detected at 90° with a photomultiplier tube. $Y_{0.6}Eu_{0.4}VO_4$ and $Y_{0.78}Yb_{0.2}Er_{0.02}VO_4$ aqueous solutions were excited at 466 nm (I_{exc} = 0.28 kW·cm^{-2}) and at 970 nm (I_{exc} = 0.55 kW·cm^{-2}), respectively. After normalization of the linear Eu^{3+} emission for the ion concentration and for the excitation intensity, the up-conversion emission of the aqueous YVO_4:Yb,Er dispersion at the excitation intensity of 0.55 kW·cm^{-2} was found to be 22 times lower than the direct emission of the YVO_4:Eu solution. Knowing that the absorption cross section, σ, of Eu^{3+} at 466 nm and of Yb^{3+} at 970 nm are, respectively, $\sigma_{Eu}(466) = 1.4 \times 10^{-21}$ cm^2[10] and $\sigma_{Yb}(970) = 10 \times 10^{-21}$ cm^2[48] and that the quantum yield of the $Y_{0.6}Eu_{0.4}VO_4$ particles, as measured with respect to a rhodamine reference, is 14%, we calculated that the quantum yield of the up-conversion emission of the $Y_{0.78}Yb_{0.2}Er_{0.02}VO_4$ solution is about 0.09 ± 0.04% at 970 nm and 0.55 kW·cm^{-2}. Given the quadratic dependence of the up-conversion emission with respect to excitation intensity (see the inset of Figure 2B), the quantum yield of up-conversion depends linearly on the excitation intensity. We, therefore, expect a quantum yield of 1.3 ± 0.5% for an intensity of 8 kW/cm^2, easily obtainable with a wide-field microscope. This value obtained in water compares favorably with the estimated value of 1% at saturation obtained on dry powder of $NaYF_4$:Yb,Er nanoparticles.[49]

Very recently, organic systems that exploit triplet-triple annihilation processes have shown a comparable up-conversion efficiency under weaker excitation power.[50,51] However, strong reduction of the up-conversion efficiency is observed in the presence of dioxygen, thus limiting biological applications in living cells.

Single-Particle Detection. Finally, we demonstrated that the up-conversion luminescence of YVO_4:Yb,Er nanoparticles is strong enough for single-particle detection. We spin-coated the YVO_4:Yb,Er nanoparticle solution on a glass coverslip, added a drop of distilled water, and observed them with an inverted wide-field microscope. The fluorescence image obtained is shown in Figure 4A. Several diffraction-limited spots are visible. We have previously shown that the nanoparticle size can be calculated from the number of photons detected per second, N_{phot}, based on the equation[10]

$$N_{phot} = q\eta\frac{\sigma I}{h\nu}4x\frac{(4/3)\pi R^3}{V} \quad (1)$$

which relates N_{phot} with the emission quantum yield q, the collection efficiency η, the absorption cross section σ, the excitation intensity I, the excitation photon energy $h\nu$, the doping fraction x, the radius of the particle R, and the unit cell volume V of the nanocrystals. In the case of $Y_{0.6}Eu_{0.4}VO_4$ particles, we have shown that particles with sizes as small as 13 nm could be detected with a wide-field microscope for an integration time of 500 ms.[10] Note that eq 1 remains valid for up-conversion emission. Indeed, introducing a quantum yield proportional to the excitation intensity leads to the number of detected photons per second being proportional to I^2.

In our microscope setup, the excitation intensity was I = 8 kW·cm^{-2} and the collection efficiency η = 0.186. As explained above, we expect the up-conversion quantum yield of $Y_{0.78}Yb_{0.2}Er_{0.02}VO_4$ particles excited with 8 kW·cm^{-2} to be q = 1.3 ± 0.5%. Using these parameters, $\sigma_{Yb}(970) = 10 \times 10^{-21}$ cm^2,[48] $h\nu$ = 1.27 eV, x = 0.2, and V = 0.323 cm^3, we can estimate from eq 1 the size of the particles giving rise to diffraction-limited spots in Figure 4A. For the particles labeled NP1, NP2, NP3, NP4, NP5, and NP6 in Figure 4A, we found a size of, respectively 10, 25, 46, 19, 31, and 30 nm, with a 15% uncertainty. These values are in good agreement with the nanoparticle size distribution found by SEM (Figure 1A). The low background signal of only a few photons allows the detection of particles emitting only a few tens of photons during the 500 ms acquisition time. Using shorter acquisition times of 50 ms, compatible with single-molecule tracking applications, nanoparticles of sizes down to 30 nm were easily observable. Even smaller sizes should be detectable with a better coupling of the excitation laser into the microscope to obtain higher excitation intensities.

Taking into account the nanoparticle size and the excitation power, this result is comparable to the one of Park et al., who succeeded in detecting single $NaYF_4$ nanoparticles with a size of 40 nm under a 150 W·cm^{-2} excitation intensity.[52] It is also

interesting to note that the excitation intensity (8 $kW \cdot cm^{-2}$) used here for this single-particle wide-field detection is orders of magnitude lower than that used in the previous confocal detection scheme (10^3 $kW \cdot cm^{-2}$).[53] It is also orders of magnitude lower than the intensities typically used for multiphoton excitation of organic fluorophores.[6] It is, in fact, almost as low as the excitation intensities used for the single-molecule observation of fluorescent proteins upon one-photon excitation[54] while being in the low-absorption NIR range instead of in the visible.

The photostability of single particles was evaluated over 8 min (Figure 4B). Neither photobleaching nor blinking was observed over this period. These features in combination with existing functionalization and coupling strategies for the YVO_4 matrix[9,10,32] mean that up-converting YVO_4:Yb,Er particles can be directly implemented for single-biomolecule tracking applications with minimal background signal.

Conclusions

Thanks to an original route for the synthesis of YVO_4 nanoparticles, we succeeded in observing up-conversion emission from an YVO_4:Er,Yb aqueous dispersion. Using a wide-field microscope, we demonstrated that individual nonblinking up-converting particles, with a size below 20 nm and covered with a water droplet, could be detected, paving the way for single-molecule imaging and tracking under NIR excitation. The possibility of exciting luminescent hydrophilic nanoparticles in the NIR range is a real breakthrough toward the development of efficient biolabels.

Although the bulk YVO_4 matrix phonons have higher energy than several fluoride matrixes, such as $NaYF_4$, an aqueous solution of YVO_4 nanoparticles shows much better up-conversion performance than $NaYF_4$ nanocrystals dispersed in water. We have thus shown that, at the nanoscale, the phonon energy of the matrix is of minor significance, with respect to the presence of crystalline defects and organic groups in and at the surface of the particles.

References and Notes

(1) Michalet, X.; Pinaud, F. F.; Bentolila, L. A.; Tsay, J. M.; Doose, S.; Li, J. J.; Sundaresan, G.; Wu, A. M.; Gambhir, S. S.; Weiss, S. *Science* **2005**, *207*, 538–544.

(2) Medintz, I. L.; Uyeda, H. T.; Goldman, E. R.; Mattoussi, H. *Nat. Mater.* **2005**, *4*, 435–446.

(3) Sargent, E. H. *Adv. Mater.* **2005**, *17*, 515–522.

(4) Larson, D. R.; Zipfel, W. R.; Williams, R. M.; Clark, S. W.; Bruchez, M. P.; Wise, F. W.; Webb, W. W. *Science* **2003**, *300*, 1434–1436.

(5) Zielinski, M.; Oron, D.; Chauvat, D.; Zyss, J. *Small* **2009**, *5*, 2835–2840.

(6) Zipfel, W. R.; Williams, R. M.; Webb, W. W. *Nat. Biotechnol.* **2003**, *21*, 1369–1377.

(7) Gamelin, D. R.; Güdel, H. U. *Top. Curr. Chem.* **2001**, *214*, 1.

(8) Auzel, F. *Chem. Rev.* **2004**, *104*, 139.

(9) Beaurepaire, E.; Buissette, V.; Sauviat, M.-P.; Giaume, D.; Lahlil, K.; Mercuri, A.; Casanova, D.; Huignard, A.; Martin, J.-L.; Gacoin, T.; Boilot, J.-P.; Alexandrou, A. *Nano Lett.* **2004**, *4*, 2079–2083.

(10) Casanova, D.; Giaume, D.; Beaurepaire, E.; Gacoin, T.; Boilot, J. P.; Alexandrou, A. *Appl. Phys. Lett.* **2006**, *89*, 253103.

(11) Masson, J.; Casanova, D.; Türkcan, S.; Voisinne, G.; Popoff, M.; Vergassola, M.; Alexandrou, A. *Phys. Rev. Lett.* **2009**, *102*, 048103.

(12) Joubert, M. F. *Opt. Mater.* **1999**, *11*, 181.

(13) Goldner, Ph.; Pellé, F. *J. Lumin.* **1993**, *55*, 197.

(14) Suyver, J. F.; Aebischer, A.; Biner, D.; Gerner, P.; Grimm, J.; Heer, S.; Kramer, K. W.; Reinhard, C.; Güdel, H. U. *Opt. Mater.* **2005**, *27*, 1111–1130.

(15) Sivakumar, S.; Diamente, P. R.; van Veggel, F. C. J. M. *Chem.—Eur. J.* **2006**, *12*, 5878.

(16) Labeguerie, J.; Dantelle, G.; Gredin, P.; Mortier, M. *J. Alloys Compd.* **2008**, *451*, 563.

(17) Vetrone, F.; Boyer, J. C.; Capobianco, J. A.; Speghini, A.; Bettinelli, M. *Chem. Mater.* **2003**, *15*, 2737.

(18) Sun, Y.; Liu, H.; Wang, X.; Kong, X.; Zhang, H. *Chem. Mater.* **2006**, *18*, 2726.

(19) Sivakumar, S.; van Veggel, F. C. J. M.; May, P. S. *J. Am. Chem. Soc.* **2007**, *129*, 620.

(20) Qui, J.; Kawamoto, Y.; Zhang, J. *J. Appl. Phys.* **2002**, *92*, 5163.

(21) Schäfer, H.; Ptacek, P.; Kömpe, K.; Haase, M. *Chem. Mater.* **2007**, *19*, 1396–1400.

(22) Heer, S.; Kompe, K.; Gudel, H. U.; Haase, M. *Adv. Mater.* **2004**, *16*, 2102.

(23) Aebischer, A.; Heer, S.; Biner, D.; Krämer, K.; Haase, M.; Güdel, H. U. *Chem. Phys. Lett.* **2005**, *407*, 124.

(24) Soukka, T.; Kuningas, K.; Rantanen, T.; Haaslathi, V.; Lörvgren, T. *J. Fluoresc.* **2005**, *15*, 513–527.

(25) Mai, H. X.; Zhang, Y. W.; Sun, L. D.; Yan, C. H. *J. Phys. Chem. C* **2007**, *111*, 13721–13729.

(26) Yi, G. S.; Chow, G. M. *Adv. Funct. Mater.* **2006**, *16*, 2324–2329.

(27) Yi, G.; Chow, G. *Chem. Mater.* **2007**, *19*, 341–343.

(28) Mialon, G.; Gohin, M.; Gacoin, T.; Boilot, J. P. *ACS Nano* **2008**, *2*, 2505–2512.

(29) Mialon, G.; Türkcan, S.; Alexandrou, A.; Gacoin, T.; Boilot, J. P. *J. Phys. Chem. C* **2009**, *113*, 18699–18706.

(30) Miller, S. A.; Caspers, H. H.; Rast, H. E. *Phys. Rev.* **1968**, *168*, 964.

(31) Casanova, D.; Giaume, D.; Moreau, M.; Martin, J. L.; Gacoin, T.; Boilot, J. P.; Alexandrou, A. *J. Am. Chem. Soc.* **2007**, *129*, 12592–12593.

(32) Giaume, D.; Poggi, M.; Casanova, D.; Mialon, G.; Lahlil, K.; Alexandrou, A.; Gacoin, T.; Boilot, J.-P. *Langmuir* **2008**, *24*, 11018–11026.

(33) Huignard, A.; Gacoin, T.; Boilot, J. P. *Chem. Mater.* **2000**, *12*, 1090.

(34) Krämer, K. W.; Biner, D.; Frei, G.; Güdel, H. U.; Hehlen, M. P.; Luthi, S. R. *Chem. Mater.* **2004**, *16*, 1244.

(35) Schäfer, H.; Ptacek, P.; Zerzouf, O.; Haase, M. *Adv. Funct. Mater.* **2008**, *18*, 2913.

(36) Pang, T.; Cao, W.; Fu, Y.; Luo, X. *Mater. Lett.* **2008**, *62*, 2500–2502.

(37) Chen, G. Y.; Zhang, Y. G.; Somesfalean, G.; Zhang, Z. G.; Sun, Q.; Wang, F. P. *Appl. Phys. Lett.* **2006**, *89*, 163105.

(38) Pires, A. M.; Serra, O. A.; Davolos, M. R. *J. Lumin.* **2005**, *113*, 174–182.

(39) Kanoun, A.; Jaba, N.; Brenier, A. *Opt. Mater.* **2004**, *26*, 79–83.

(40) Dantelle, G.; Mortier, M.; Patriarche, G.; Vivien, D. *J. Solid State Chem.* **2006**, *179*, 2005.

(41) Dantelle, G.; Mortier, M.; Patriarche, G.; Vivien, D. *Chem. Mater.* **2005**, *17*, 2216–2222.

(42) Capobianco, J. A.; Kabro, P.; Ermeneux, F. S.; Moncorgé, R.; Bettinelli, M.; Cavalli, E. *Chem. Phys.* **1997**, *214*, 329–340.

(43) Buissette, V.; Huignard, A.; Gacoin, T.; Boilot, J. P.; Aschehoug, P.; Viana, B. *Surf. Sci.* **2003**, *532−533*, 444–449.

(44) Page, R. H.; Schaffers, K. I.; Waide, A. P.; Tassano, J. B.; Payne, S. A.; Krupke, W. F. *J. Opt. Soc. Am. B* **1998**, *15*, 996–1007.

(45) Etchart, I.; Huignard, A.; Bérard, M.; Nordin, M. N.; Hernandez, I.; Curry, R. J.; Gillin, W. P.; Cheetham, A. K. *J. Mater. Chem.* **2010**, *20*, 3989–3994.

(46) Casanova, D.; Giaume, D.; Gacoin, T.; Boilot, J.-P.; Alexandrou, A. *J. Phys. Chem. B* **2006**, *110*, 19264.

(47) Casanova, D.; Bouzigues, C.; Nguyen, T. L.; Ramodiharilafy, R. O.; Bouzhir-Sima, L.; Gacoin, T.; Boilot, J. P.; Tharaux, P. L.; Alexandrou, A. *Nat. Nanotechnol.* **2009**, *4*, 581–585.

(48) Tsuboi, T. *Phys. Rev. B* **2000**, *62*, 4200–4203.

(49) Yi, G.; Lu, H.; Zhao, S.; Ge, Y.; Yang, W.; Chen, D.; Guo, L. H. *Nano Lett.* **2004**, *4*, 2191–2196.

(50) Monguzzi, A.; Mezyk, J.; Scotognella, F.; Tubino, R.; Meinardi, F. *Phys. Rev. B* **2008**, *78*, 195112.

(51) Auckett, J. E.; Chen, Y. Y.; Khoury, T.; Clady, R. G. C. R.; Ekins-Daukes, N. J.; Crossley, M. J.; Schmidt, T. W. *J. Phys.: Conf. Ser.* **2009**, *185*, 012002.

(52) Park, Y. I.; Kim, J. H.; Lee, K. T.; Jeon, K. S.; Na, H. B.; Yu, J. H.; Kim, H. M.; Lee, N.; Choi, S. H.; Baik, S. I.; Kim, H.; Park, S. P.; Park, B. J.; Kim, Y. W.; Lee, S. H.; Song, I. C.; Moon, W. K.; Suh, Y. D.; Hyeon, T. *Adv. Mater.* **2009**, *21*, 4467–4471.

(53) Wu, S.; Han, G.; Milliron, D. J.; Aloni, S.; Altoe, V.; Talapin, D. V.; Cohen, B. E.; Schuck, P. J. *Proc. Natl. Acad. Sci. U.S.A.* **2009**, *106*, 10917.

(54) Harms, G. S.; Cognet, L.; Lommerse, P. H. M.; Blab, G. A.; Kahr, H.; Gamsjäger, R.; Spaink, H. P.; Soldatov, N. M.; Romanin, C.; Schmidt, T. *Biophys. J.* **2001**, *81*, 2639–2646.

JP107900Z